UNIVERSITY OF CALIFORNIA
RIVERSIDE

Measurement of Fine Particles From Mobile and Stationary Sources, and Reducing the Air Conditioner Power Consumption in Hybrid Electric Vehicles

A Thesis submitted in partial satisfaction
of the requirements for the degree of

Master of Science

in

Mechanical Engineering

by

Eli Henry Brewer

June 2015

Thesis Committee:

Dr. Heejung Jung, Chairperson
Dr. David Cocker
Dr. Akula Venkatram

The Thesis of Eli Henry Brewer is approved:

Committee Chairperson

University of California, Riverside

Acknowledgements

The text of this thesis, in part, is a reprint of the material that is in review for publication for Atmospheric Environment. The co-author Heejung Jung listed in that publication directed and supervised the research which forms the basis for this thesis. Yang Li helped sample data, and write the report to AQMD, Bob Finken was the head of the DELTA team who performed the $PM_{2.5}$ and gaseous sampling and analysis, Greg Quartucy was the primary go-between for WCEP, SCAQMD, UCR and DELTA, and was overall project lead, Lawrence Muzio was the FERCo supervisor, Al Baez was an SCAQMD supervisor, and Mike Garibay was an SCAQMD supervisor.

Thank you, Heejung for introducing me to this field and for giving me opportunity to work in it. Thank you to my committee members David Cocker and Akula Venkatram, and co-authors Yang Li, Bob Finken, Greg Quartucy, Lawrence Muzio, Al Baez, Mike Garibay, and Heejung Jung. Thank you Mike Grady for mentoring me and for adventures in the heat of the Mojave.

Thank you Jason McMillan, Matt Gross, Molly Daniels, Tim Beck, Sara Henry, Megan Rohrssen for bike rides, and preserving sanity. Thank you Howard and Kim Brewer for the gifts I was born with and the inquisitiveness you taught me. Thank you Jacqui Gilchrist for the constant support, and for editing everything.

ABSTRACT OF THE THESIS

Measurement of Fine Particles From Mobile and Stationary Sources, and Reducing the Air Conditioner Power Consumption in Hybrid Electric Vehicles

by

Eli Henry Brewer

Master of Science, Graduate Program in Mechanical Engineering
University of California, Riverside, June 2015
Dr. Heejung Jung, Chairperson

We study the $PM_{2.5}$ and ultrafine exhaust emissions from a new natural gas-fired turbine power facility to better understand air pollution in California. To characterize the emissions from new natural gas turbines, a series of tests were performed on a GE LMS100 gas turbine. These tests included $PM_{2.5}$ and wet chemical tests for SO_2/SO_3 and NH_3, as well as ultrafine (less than 100 *nm* in diameter) particulate matter measurements. The turbine exhaust had an average particle number concentration that was $2.3x10^3$ times higher than ambient air. The majority of these particles were nanoparticles; at the 100 *nm* size, stack particle concentrations were about 20 times higher than ambient and increased to $3.9x10^4$ times higher on average in the 2.5 - 3 *nm* particle size range. This study also found that ammonia emissions were higher than expected, but in compliance with permit conditions. This was possibly due to an ammonia imbalance entering the catalyst, some flue gas bypassing the catalyst, or not enough catalyst volume. SO_3 accounted for an average of 23% of the total sulfur oxide emissions measured. Some of the SO_3 is formed in the combustion process and it is likely that the majority formed as the SO_2 in the

combustion products passed across the oxidizing CO catalyst and SCR catalyst. The 100 *MW* turbine sampled in this study emitted particle loadings similar to those previously measured from turbines in the SCAQMD area, however, the turbine exhaust contained far more particles than ambient air.

The power consumed by an air conditioner accounts for a significant fraction of the total power used by hybrid and electric vehicles, especially during summer. This study examined the effect of recirculation of cabin air on power consumption of mobile air conditioners, both in-lab and on-road. An On Board Diagnostic monitor recorded real time power consumption and vehicle mileage, and fuel economy was measured by the carbon balance method. Vehicle mileage improved with increased cabin air recirculation. The recirculation of cabin air also significantly reduced in-cabin particle concentrations. Recirculation of cabin air was determined to be an excellent and immediate solution to increase vehicle mileage and improve cabin air quality.

Contents

List of Figures ix

List of Tables xi

Forward 1

Chapter 1 $PM_{2.5}$ and Ultrafine Particulate Matter Emissions from Natural Gas-Fired Turbine for Power Generation 2

1. Introduction 2

2. Experimental 5

2.1 Test Site, turbine, fuel, and lubricant 5

2.2 Measurement setup 7

2.2.1. Ultrafine particle measurement setup 7

2.2.2 $PM_{2.5}$ Measurement Setup 9

2.2.3 Gas Measurement setup 9

3. Results and Discussion 10

3.1 Particle size distributions and morphology 10

3.2 $PM_{2.5}$ measured by the method 201A/5.1 17

3.3 Gaseous Emissions 19

4. Discussion and Conclusion 21

Chapter 2 Reducing Mobile Air Conditioner Power Consumption Using Active Cabin Air Recirculation in Hybrid Electric Vehicles 23

1. Introduction 23

2. Experimental 25

2.1 Instruments 25

2.2 Vehicles 27

2.3 Tests 28

2.3.1 On-Road Test Route 28

2.3.2 Laboratory Test SC03 30

2.3.3 Highway 33

2.4 Calculating Fuel Economy 33

3. Results 35

3.1 SC03 Driving Cycles 35

3.2 On-Road 36

3.3 In-Cabin Air Quality 38
4. Conclusions 39
References: 41
Appendix A: Parameter Identifiers used to query the OBD-II 45

List of Figures

Figure 1: WCEP Unit 2 Stack Diagram. Note samples were collected near the top of the exhaust stack after well after the catalyst and ammonia injection. Stack overall inside diameter is 13’6”. Overall stack height is 90’0”. [15] 6

Figure 2: Experimental setup diagram, the Catalytic Stripper was used only on certain tests, and when it was not used the SMPS received a direct line from the diluted sample. It should be noted that a thermophoretic TEM sampler was used to directly sample stack flow. 7

Figure 3: Particle size distributions from the stack of the turbine engine in comparison to those from ambient air. Note peak from 2-5 nm and overall higher particle counts than ambient air. 11

Figure 4: TEM images of sampled particles from Unit 2 by Thermophoretic TEM sampler (a) Day 6 (b) Day 7 (c) Day 8 (d) Day 9. Note the low contrast is indicative of non-metals, and the particle sizes observed in the TEM match the particle size distribution in figure 3. 14

Figure 5: EAD Aerosol diameter concentration vs varying turbine load. Note that surface area concentration follows turbine load although with some delay. 16

Figure 6: PM2.5 Measured using SMPS, Methods 201A/5.1 & 201A/202. Note that the SMPS calculated result is of the same order of magnitude as that of method 5.1. 17

Figure 7: Average Contribution of Ion to Condensable Inorganic PM2.5 Mass Measured Using Method 201A/5.1 from the AAC Laboratory. Note that sulfate makes up the largest portion of ions followed by undetermined and ammonium. 19

Figure 8: On-Road Charge Depletion Route 3.34 Miles. Map created with GPSVisualizer.com using ArcGIS World topo [59] 29

Figure 9: Average Speed Plot On-Road Route. The relatively low variability of the speed indicates that our testing was highly repeatable. 30

Figure 10: FTP SC03 driving cycle speed plot used for in-lab chassis testing of the Prius. It is designed to simulate the rapid braking and accelerations that are seen in real-world driving. It also utilizes the air conditioner. [54] 30

Figure 11: Example speed plot from day 2 of testing. Each peak is the middle of a single SC03 test. 31

Figure 12: Example of best controlled in-lab temperature for set of three SC03 driving cycle tests. ACO heats cabin back up to within 1 °C of pre-ACF test. 32

Figure 13: VERL vs. OBDII fuel economy. Highly reliable OBDII data shows that the OBD data is an appropriate tool for measuring fuel economy. 35

Figure 14: AC Energy consumption. All data shows increasing trend with temperature as is expected for the MAC to cool the cabin more. On-road data reduced consumption likely implemented by Toyota to improve EV range..... 36

Figure 15: Fuel Economy from all tests calculated from the OBDII. Separation of on-road and in-lab data indicated how the Prius operates differently under different driving modes. The Leaf fuel economy is in the range of the Prius' fuel economy. 37

Figure 16: CO_2 Clear Test from recirculate to fresh air. Ambient CO2 concentration levels were achieved within 1 minute of switching from recirculate to fresh air. 38

Figure 17: Normalized histograms of highway EAD data. ACR reduces particle concentrations in the vehicle cabin. In-cabin air quality is significantly improved by the reduction of particles, while CO2 increases tenfold after 35 min., particles reduce tenfold after only 16 min. Ambient data is from a similar trip on the 91 fwy. in July by Liem Pham. 39

List of Tables

Table 1: Summary of PM2.5 Emissions Measurements Method 201A/5.1. Note the majority of the $PM_{2.5}$ is condensable and inorganic..... 17

Table 2: Summary of Gaseous Emissions, Ammonia Slip Measurements, & SO2/SO3 (Daily data can be seen in the supplementary files) 20

Table 3: Toyota Prius Plug-in and Nissan Leaf selected Specifications 28

Table 4: List of On Board Diagnostic Parameter IDs (PID) used in testing. Mode 21 signifies a Toyota defined PID. Letters represent the location of the value in OBD-II output [58] 45

Forward

This thesis is comprised of two separate journal papers that are wholly unrelated and are presented here as two separate chapters. The first chapter is a study of particulate matter less than 2.5 μm ($PM_{2.5}$) and ultrafine emissions from a new natural gas-fired turbine. The second chapter investigates improvements in the fuel economy of hybrid electric vehicles by recirculating cabin air, and how air recirculation impacts in-cabin air quality.

Chapter 1

$PM_{2.5}$ and Ultrafine Particulate Matter Emissions from Natural Gas-Fired Turbine for Power Generation

Eli Brewer[1], Yang Li[1], Bob Finken[2], Greg Quartucy[3], Lawrence Muzio[3], Al Baez[4], Mike Garibay[4], Heejung S. Jung[1]

[1]University of California Riverside (UCR), Department of Mechanical Engineering, Riverside, CA 92521

[2]Delta Air Quality Services, Inc. 1845 North Case Street Orange, CA 92865

[3]Fossil Energy Research Corporation (FERCo), 23342-C South Pointe Dr. Laguna Hills, CA 92653

[4]South Coast Air Quality Management District (SCAQMD), 21865 Copley Dr. Diamond Bar, CA 91765

1. Introduction

Natural gas turbines (NGTs) are critical for meeting the demand of U.S. electrical power generation because they are uniquely suited to fulfill the energy gap left by hydroelectric, nuclear, and renewable energy sources. NGTs have a relatively quick start-up and shut-down time compared to other sources of electricity, making them ideal for supplying energy to the grid when the demand changes rapidly. New shale gas mining techniques have lowered the price of natural gas and allowed greater access to the United States' shale gas resources. The overnight capital cost (the cost of the project if no

interest were accrued during its construction) of a NGT is low compared to other electrical generating sources [1] and can be rapidly installed to cover unexpected situations like the shutdown of the San Onofre Nuclear Generating Station (SONGS) [2].

Since 2003 California has seen an increase of over 200% in electrical generation from natural gas [3]. The decreasing price and stable domestic supply of natural gas have strongly influenced its increased use [4], and the use of NGTs has been projected to increase until at least 2040 [5]. Studying the exhaust from these new facilities is critical to our understanding of air pollution in California.

Several groups have studied particulate Matter (PM) emissions from NGTs. England et al. [6] investigated a compact dilution sampler (CDS) methodology to characterize fine particle emissions from stationary sources including one NGT. They found that the CDS method had lower detection limits compared to the regulatory methods for PM emissions. Tamura [7] recently conducted a gap analysis of the filterable and condensable PM emission factors from stationary external and internal combustion sources fired by gaseous and liquid fuel to evaluate the accuracy of the sampling methodology. PM emission studies have covered many of the power plant combustors, however, there is still only limited research on emissions from aeroderivative turbines burning natural gas. Each fuel type emits a distinct chemical composition and particle range, based on combustion characteristics and the chemical nature of the fuel [8–10]. Current U.S. E.P.A. regulations measure $PM_{2.5}$ emissions using mass based methods, however, larger particles, which are usually generated by incomplete combustion, make up a much higher mass fraction than ultrafine particles [11]. Fine particles make up the

majority of the number fraction of particles, but the EPA has not separately regulated ultrafine PM (particles < 100 *nm* in diameter). NGTs emit a wide range of particles therefore the majority of particles emitted are not regulated effectively.

Ultrafine particles have recently become a cause for concern, as our understanding of their effect on the human body has improved. They are hypothesized to have increased health risks compared to larger particles due to their higher lung deposition rate, the ineffectiveness of the human body's clearance mechanism for them, and their ability to translocate to extra-pulmonary locations, e.g. the lymphatic and circulatory systems [12]. However, the health effects of breathing in ultrafine PM remain uncertain. A 2013 report from the Health Effects Institute on the toxicity of ultrafine PM (outside of effects from all $PM_{2.5}$) was inconclusive due to inconsistencies in the findings of the short-term studies, and lack of long-term exposure studies [13].

SCAQMD funded a two-stage project to technically and economically assess a variety of control strategies and technologies that could potentially be used to reduce $PM_{2.5}$ and ultrafine emissions from NGT power plants. In 2007, SCAQMD amended rule 1309.1 to allow prospective gas turbine-based power plants conditional access to its Priority Reserve account to procure reduction credits to offset $PM_{2.5}$ emissions. At the same time, SCAQMD initiated a project to identify and test, at pilot scale, advanced $PM_{2.5}$ technologies to reduce emissions from these gas turbine-based power plants. The first phase [14] of this project entailed an assessment of technologies to reduce $PM_{2.5}$ and ultrafine particles from gas turbine engines; the second phase [15] of the project entailed pilot scale evaluations of technologies recommended from the first phase. This paper

reports part of the results from the second phase of the project with the main objective of characterizing and quantifying $PM_{2.5}$ and ultrafine particles that are emitted by modern aeroderivative NGTs during daily operation. The $PM_{2.5}$ test methods selected for this project were chosen from currently available methods. SCAQMD Method 5.1 [16] combined with EPA Method 201A [17] were chosen as the test methods because recent projects in the SCAQMD jurisdiction have utilized this combination of methods for the determination of $PM_{2.5}$ including condensable PM. Methods 5.1/201A are detailed in section 2.2.2.

2. Experimental

2.1 Test Site, turbine, fuel, and lubricant

Tests were conducted at the Walnut Creek Energy Park (WCEP) in the City of Industry, CA in August 2013. The test site was selected because it was representative of new aeroderivative turbines and had the newest commercial NO_x control system. WCEP was designed as a peaking plant to provide electrical generation during high demand periods, i.e. Southern California's hot summer months.

WCEP consists of five GE LMS100 combustion turbines in simple cycle operation. The LMS100 is an aeroderivative gas turbine rated nominally at 100 *MW* [18]. The LMS100 derives its high efficiency and increased power output from its innovative intercooling system between the low-pressure and high-pressure compressors. WCEP uses reclaimed water for cooling; each LMS100 employs Selective Catalytic Reduction (SCR) system (from Haldor-Topsoe), using aqueous ammonia as the reagent, and water

injection for NO_x control. They are also equipped with a CO catalyst (from BASF). The test unit for this study was WCEP Unit 2 and its exhaust layout is shown in figure 1.

Specific fuel analysis was not performed for this study. In general, the average Wobbe number for California pipeline natural gas is in the range of 1335-1340 *Btu/scf* with sulfur content in the range of 0.25-1 *grain/100scf [19]*. The LMS100s at WCEP uses two types of oil: Mobil DTE Light lubrication oil and Mobil Jet Oil II.

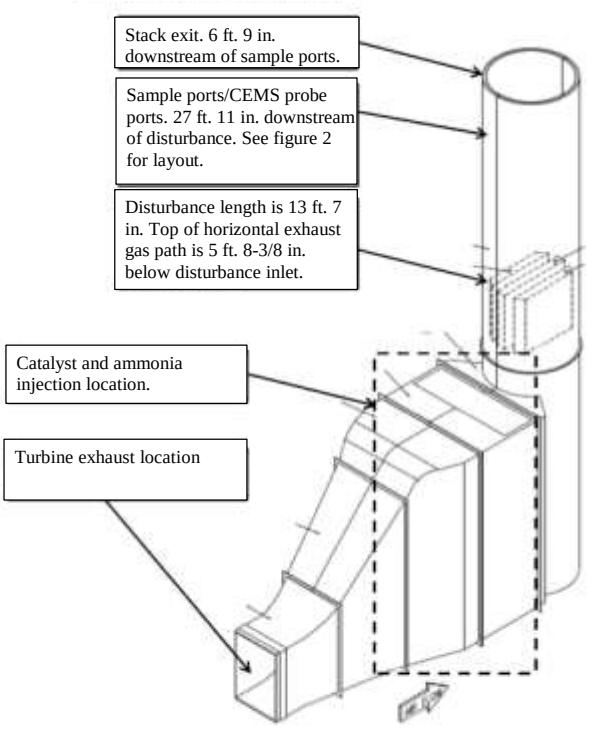

Figure 1: WCEP Unit 2 Stack Diagram. Note samples were collected near the top of the exhaust stack after well after the catalyst and ammonia injection. Stack overall inside diameter is 13'6". Overall stack height is 90'0". [15]

The ultrafine PM tests were conducted before turbine operation, during plant warm-up, and during normal operation. A record was kept of which turbines were running to track how ambient conditions changed with energy park operation. WCEP is located adjacent to a train yard, and the associated diesel locomotive traffic influenced the ambient conditions. Energy park operation is controlled by Southern California Edison (SCE) and is dictated by the demand on the electrical grid.

2.2 Measurement setup

2.2.1. Ultrafine particle measurement setup

Samples were pulled from the middle of the stack through an unheated, uninsulated, 3/8" stainless steel tube inserted into a sample port that was located on the side of the stack above platform. The sample probe was connected via silicon conductive tubing to a critical orifice (maintaining a dilution ratio of 7.1:1) upstream of an ejector pump (Air-Vac, model TD110H). A dilution tunnel was connected downstream of the ejector pump to mix the dilution air with the sample [20]. Compressed air (maintained at 30 *psi*) was supplied by the power plant and filtered to particle free air by a clean air system (TSI model 3074). The ultrafine measurement setup (seen in figure 2) had the sample passing through the dilution tunnel to the SMPS (TSI model 3936), EAD (TSI model 3070A), Transmission Electron Microscope (TEM) sampler, and Catalytic Stripper (CS). The thermophoretic TEM sampler directly sampled the turbine exhaust. The CS was connected in-line, before the SMPS, during part of the tests to determine what portion of the sample was made of Volatile Organic Compounds (VOCs).

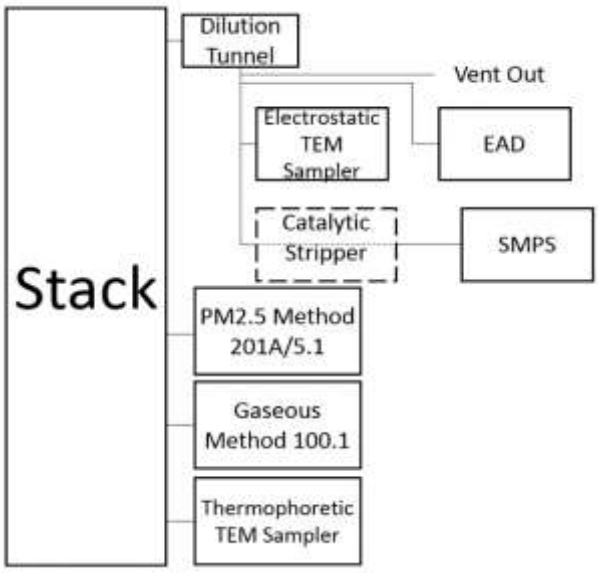

Figure 2: Experimental setup diagram, the Catalytic Stripper was used only on certain tests, and when it was not used the SMPS received a direct line from the diluted sample. It should be noted that a thermophoretic TEM sampler was used to directly sample stack flow.

Two types of classifiers were used for the SMPS: the long column DMA (model 3081) sampled over a range of 7 *nm* to 290 *nm*, and the Nano DMA (model 3085) sampled over a range of 2.5 *nm* to 80 *nm*. The SMPS used an ultrafine Condensation Particle Counter (TSI, CPC 3776), which has a cut point of 2.5 *nm*. Due to the warm ambient temperatures during the test, the CPC was placed in a small cardboard box where a portable air conditioner supplied cool air. This was necessary to keep the CPC's condenser temperature below its operating maximum.

Two types of samplers were used to collect particles on TEM grids. The thermophoretic sampler was inserted into the stack with a residence time of a fraction of a second. A guiding tube was used so that the TEM grids were only exposed to particles in the stack. This is the same thermophoretic sampler used by Murphy et al. [21]. The electrostatic particle sampler (FHNW TEM Sampler, Switzerland) was also used to collect particle samples after the sample flow was diluted. Typical sampling time ranged from 30 – 120 minutes for the electrostatic particle sampler. Both Silicon Oxide (SiO) and Carbon coated 200 mesh copper grids were used.

A custom built CS (similar in design to Abdul-Khalek and Kittelson[22], and Stenitzer [23]) was used in-line upstream of the SMPS to measure the fraction of the PM that were Volatile Organic Compounds (VOCs). The CS has two catalysts that are heated to 300 *°C*: the first oxidizes hydrocarbon components (Oxicat) and the second removes sulfur components (S-trap) from the sample flow. The sample flow passes through a cooling coil to decrease the flow to ambient temperature before exiting the CS. A flow

rate of 1.5 *lpm* was used to match the flow rate of the SMPS. Additionally, both wall and diffusion losses were accounted for.

The EAD detects diameter concentration load using the principle of diffusion charging. It then calculates the concentration based on a TSI propriety linear relationship. Diameter concentration is correlated with the degree that tracheobronchial and alveolar regions have been covered by ultrafine particles. [24,25]

2.2.2 $PM_{2.5}$ Measurement Setup

$PM_{2.5}$ was measured using both U.S. EPA/SCAQMD method 201A/5.1 and U.S. EPA method 201A/202 for the SCAQMD project. This paper mainly reports results by method 201A/5.1, however, the full report contains other methods that are outside the scope of this paper. For more details see figure S3.

2.2.3 Gas Measurement setup

NO_x, CO, O_2 and CO_2 concentrations were measured using SCAQMD Method 100.1 using a dry extractive continuous emissions monitoring (CEM) system. The CEM has a heated probe, which is a heat traced Teflon sample line connected to a thermo-electrically cooled sample dryer to minimize loss of NO_2. The gas analysis portion is composed of a chemiluminescent NO_x analyzer (CAI Model 600), a gas filter correlation CO analyzer (Thermo-Fisher Model 48i), an electrochemical O_2 analyzer (AMI Model 201), and a non-dispersive infrared CO_2 analyzer (Horiba Model PIR-2000). A low

temperature carbon converter was used to convert NO_2 to NO for measurement of total NO_x and converter efficiency was tested daily.

The ammonia slip (the amount of ammonia that escapes the SCR system unreacted) was measured using SCAQMD Method 207.1 (shown and detailed in figure S1). NCASI Method 8A was used to measure the concentrations of SO_2 and SO_3 (see and detailed figure S2).

3. Results and Discussion

3.1 Particle size distributions and morphology

The average SMPS results, using both the Long and Nano DMA columns, are shown in figure 3. Ambient particle size distributions are shown as averages of five test days and turbine exhaust particle size distributions are the averages of two test days. Due to the relatively low dilution ratio, the sampling condition was close to the ion depletion condition of the bipolar neutralizer on the SMPS. The data were screened to ensure that the measurements presented in this paper were not conducted under the ion depletion condition. Averaged data are also provided in figure S4. The SMPS data shows good agreement over the range of overlap between 7 *nm* and 80 *nm*. The particle size distribution of the exhaust showed a bimodal distribution, with peaks around 2.8 *nm* and 17 *nm*. The ultrafine emissions from the stack were at least an order of magnitude higher than ambient air over the entire size range. At the 100 *nm* size, stack particle concentrations were 20 times higher than ambient particle concentrations. This increased

to an average of $3.9x10^4$ times higher in the 2.5 *nm* - 3 *nm* range. Overall, stack particle concentrations were over $2.3x10^3$ times higher than ambient particle concentrations. Total ambient particle concentrations were in the range of $2x10^4$ *#/cc*, which is higher than typical background particle concentration in the region.

Nguyen et al [26] has reported 8000-10,000 *#/cc* for a background location in Riverside, while others have reported higher concentrations of 10,000-100,000 *#/cc* for measurements taken near a major highway [27,28]. Ambient particle concentrations are higher than expected for an urban area and this is attributed to the close proximity (less than a kilometer) of a major highway (California State Route 60) and the adjacent train yard. The results of our study contradict what Klippel et al. [29] reported that gas-fired turbine exhaust particle concentrations were lower than those of ambient air. They found similar results for both 260 *MW* and 7.9 *MW* turbines. The 260 *MW* turbine has water injection for NO_x control, similar to the turbine sampled in this study. They did not

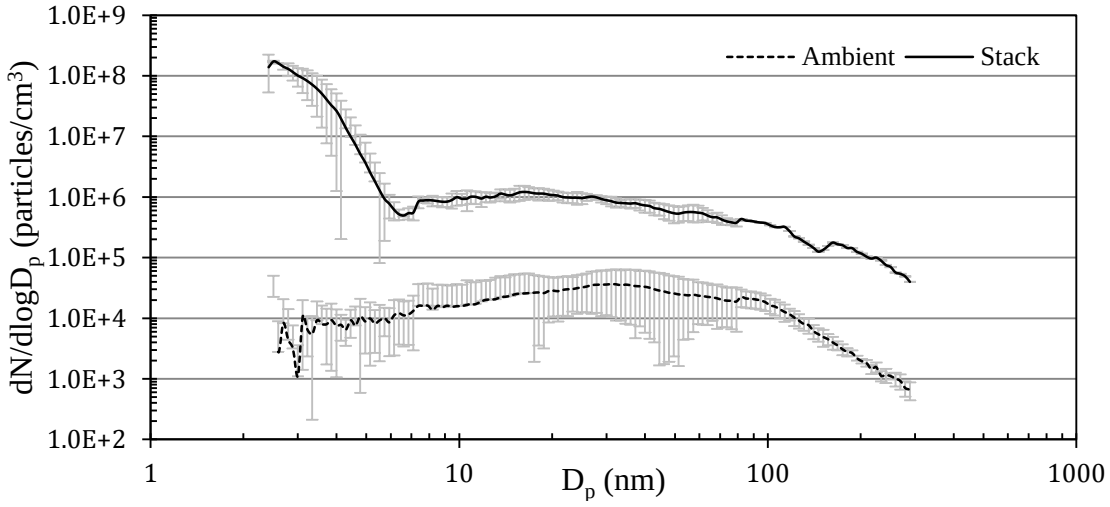

Figure 3: Particle size distributions from the stack of the turbine engine in comparison to those from ambient air. Note peak from 2-5 nm and overall higher particle counts than ambient air.

measure particles below 10 *nm,* therefore the presence of nanoparticles in the exhaust of their turbines cannot be ruled out. Their particle size distributions show significantly lower accumulation mode (> 30 nm in diameter) particle concentrations than those in this study. We speculate that the post combustion temperatures of their turbines were much higher than those of the turbine sampled in this study, leading to further oxidation or gasification of accumulation mode particles. Information on the sulfur content of the fuel could provide an improved explanation of nucleation mode particles (< 30 *nm* in diameter), however, neither of the studies measured fuel sulfur content.

The CS was inserted between the dilution tunnel and the SMPS to remove semi-volatiles and sulfur compounds from the aerosol sample streams in order to quantify the amount of VOCs in the exhaust. The fraction of particles that were semi-volatile can be determined from the difference between cold and hot particle counts (accounting for thermophoretic and diffusion losses). Thermophoretic losses are less dependent on particle size than diffusion losses (for particle sizes between 10 *nm* and 100 *nm).* Size independent thermophoretic losses were not observed in our measurements for particles between 10 *nm* - 40 *nm*. We assume that a fraction of the 100 *nm* particles were semi-volatile because of the lower particle counts measured from the hot CS in that size range (see figure S5). Further study is required to confirm this observation due to a lack of robust CS test data and high diffusion losses within the CS.

Studies have investigated particle size distributions from combustion sources and have found a variety of factors that impact the shape of the distribution. Gysel et al. [30] varied the dilution conditions (temperature, humidity, and residence time) of nucleation

mode particles from a NGT and showed that they were highly hygroscopic, and sulfur compounds in the exhaust, combined with the various dilution conditions, could significantly affect the peak diameter of the particles. Other studies showed that aircraft turbine (burning jet fuels) emissions showed different particle size distributions compared to our study. Lobo et al. [31] reported unimodal particle size distributions with the mode diameters ranging from 20 *nm* to 30 *nm*, while Herndon et al. [32] reported bimodal particle size distributions with the mode of the nucleation mode around 10 *nm* and the larger peak in the 40 *nm* - 70 *nm* range. England and McGrath [33] reported particle size distributions, measured by SMPS, from a 48 *MW* aeroderivative cogeneration turbine (burning refinery fuel), yet their distribution was not dilution corrected. Chang and England [34] showed particle distribution measured by SMPS, and PM measured by Method 201A and 202, of a 234 *kW* pilot scale combustion facility, however this turbine is significantly different from the aeroderivative turbine in this study. Wien et al. [35] and England et al. [36] used methods 201A and 202 to measure PM from 240 *MW* and 554 *MW* cogenerative supplementary-fired natural gas, combined cycle power plants, however, this is also a different type of turbine. England et al. [6] found that both the residence time of particles and the dilution ratio of the sample flow to dilution air affect the particle distribution from burning natural gas, however these changes were all within the same order of magnitude. These previous studies are distinctly different from this study and thus our results cannot be directly compared.

This study found significant concentrations of nanoparticles with a smaller peak diameter than those found in the emissions from jet fuels. Despite the relatively short

lifetime of nanoparticles in the atmosphere (minutes to hours), they can become a concern for public health when they coagulate onto accumulation mode particles, which have lifetimes on the order of days [37].

TEM samples were taken to study the morphology and chemical composition of particles emitted from the turbine. These grids were analyzed on a Philips CM300 TEM at UCR's Central Facility for Advanced Microscopy and Microanalysis (CFAMM). Four TEM images of the particles are shown in figure 4. There is a consistently dominant presence of 2-3 *nm* diameter particles due to the significantly higher concentration (four orders of magnitude) of nanoparticles in the turbine exhaust. Although a few larger particles were observed, they were not photographed due to our greater interest in the smaller particles. Energy-dispersive X-ray spectroscopy (EDX) analysis was inconclusive because the volume of nanoparticles was small and the signal to noise ratio was low. The low contrast particles shown in figure 4 are assumed to be non-

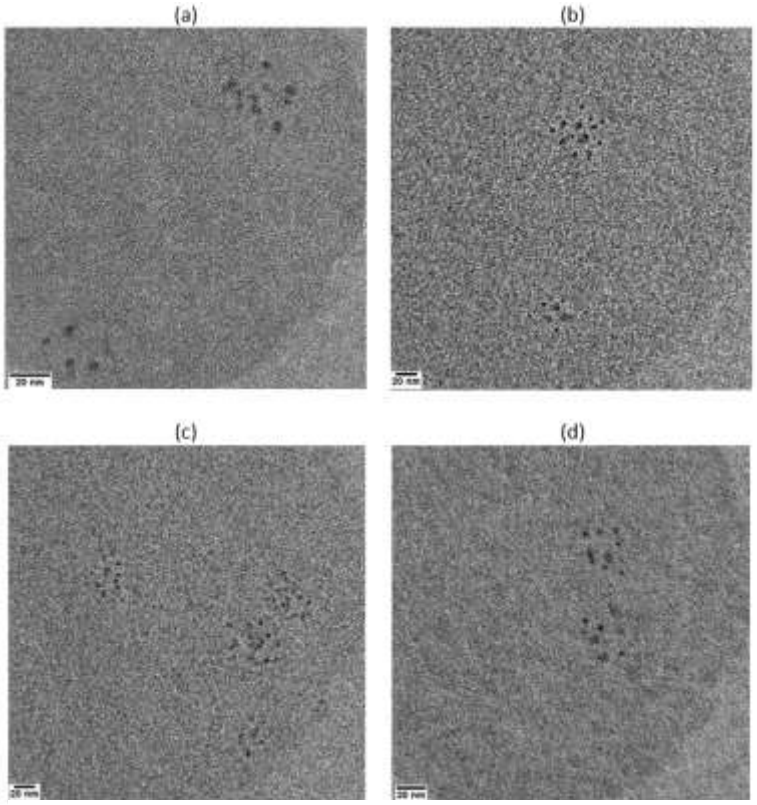

Figure 4: TEM images of sampled particles from Unit 2 by Thermophoretic TEM sampler (a) Day 6 (b) Day 7 (c) Day 8 (d) Day 9. Note the low contrast is indicative of non-metals, and the particle sizes observed in the TEM match the particle size distribution in figure 3.

metallic because metallic particles typically have high contrast in TEM images. It is unlikely that the particles seen on the TEM grids were semi-volatile due to the presence of a CO catalyst in the turbine (the CO catalyst is designed to remove hydrocarbons, much like our CS). Further testing is nesseccary to determine their exact chemical composition and formation process.

The particle mass concentration was estimated based on the particle size distribution. Two different effective density profiles for particles were used (shown in figure S6). Initially, a constant density of 1 g/cm^3 was used (assuming a spherical particle shape). Most organic aerosols have densities in the range from 1.22 g/cm^3 to 1.43 g/cm^3 [38,39], while representative particle phase inorganics (e.g. ammonium nitrate and ammonium sulfate) have densities of 1.72 g/cm^3 and 1.77 g/cm^3 respectively. The effective density distribution from Maricq and Xu [40] was utilized for accumulation mode particles as shown in Equation 1. A density of 1.46 g/cm^3 (equal to that of hydrated sulfuric acid) was assumed following Zheng et al.'s [41] calculation for nucleation mode particles.

$\rho_{eff} = 1.2378 * e^{-0.048 D_p}$ *(D_p>30* nm*)* *Equation. 1*

Integration of the particle mass, obtained from each size bin, yielded an ambient PM mass of 5.7 $\mu g/m^3$ (for a constant density of 1 *g/cc),* and 4.0 $\mu g/m^3$ (for the complex density profile). Our calculation was similar to the air quality index (AQI) reported during the test days (49 +/- 2.7, or11.75 +/- 0.57 $\mu g/m^3$).

The CPC and EAD were used to monitor changes in particle number and diameter concentration during the load variations (see Table S1 for operating data summary and

details). The CPC periodically counted sample flow (bypassing the SMPS), however the sample flow often surpassed the instrument's concentration limit because of the high particle concentration of the turbine exhaust, so useful monitoring data could not be obtained. The EAD recorded the transient response of particle emissions from the stack during the load variations (figure 5). While particle emissions decreased with no time-delay when the load decreased from 100 *MW* to 50 *MW*, there was a 10 - 15 minute time-delay when the load was increased from 50 *MW* to 100 *MW*. There were spikes in the particle concentration when the turbine operated at either 50 *MW* or 100 *MW*. It should be noted that the EAD has low penetration and charging efficiencies for particles below 10 *nm*, however we speculate that the EAD may have responded to sub-10 *nm* particles because of the high concentrations recorded.

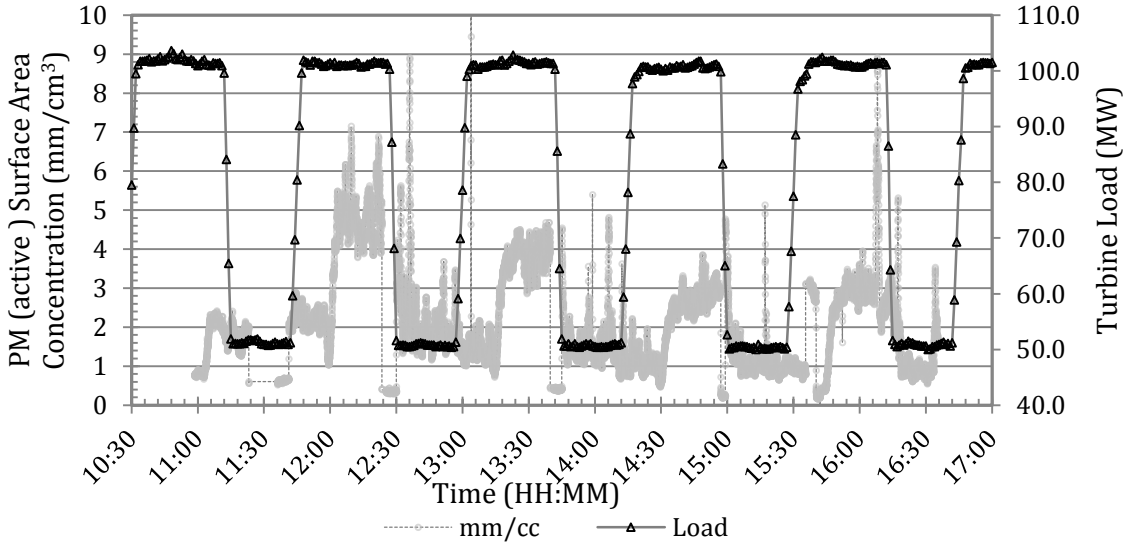

Figure 5: EAD Aerosol diameter concentration vs varying turbine load. Note that surface area concentration follows turbine load although with some delay.

3.2 $PM_{2.5}$ measured by the method 201A/5.1

The loading of $PM_{2.5}$ in the exhaust, measured using Method 201A/5.1 (Table 1), was 0.000296 *grain/dscf (*677 $\mu g/m^3$). Of the total $PM_{2.5}$: 8.1% (55µg/m^3) was condensable organic PM, 84.8% (574µg/m^3) was condensable inorganic PM, and 7.1% (48µg/m^3) was solid $PM_{2.5}$ (figure 6). The PM mass estimated from particle size distributions (assuming a unit density) was 200 $\mu g/m^3$, and is similar to the 654 $\mu g/m^3$ of PM measured by the Method 201A/5.1.

Table 1: Summary of PM2.5 Emissions Measurements Method 201A/5.1. Note the majority of the $PM_{2.5}$ is condensable and inorganic.

	PM loading, gr/dscf (µg/m^3)	Percent of Total PM
Solid PM > 2.5 micons	2.30E-05 (52.63)	
Solid PM < 2.5 micons	2.10E-05 (48.06)	7.1%
Condensable Inorganic PM < 2.5 micons	2.51E-04 (574.37)	84.8%
Condensable Organic PM < 2.5 micons	2.40E-05 (54.92)	8.1%
Toal PM < 2.5 micons	2.96E-04 (677.35)	

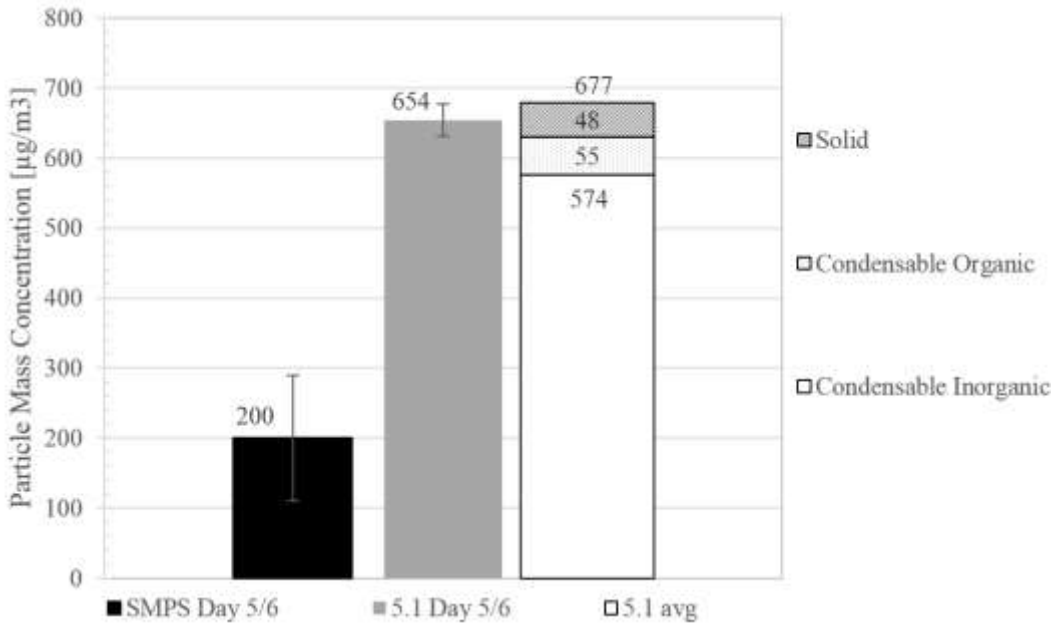

Figure 6: PM2.5 Measured using SMPS, Methods 201A/5.1 & 201A/202. Note that the SMPS calculated result is of the same order of magnitude as that of method 5.1.

Ionic analyses were performed for seven anions (sulfate, chloride, fluoride, nitrite, nitrate, bromide, and phosphate) and six cations (ammonium, calcium, lithium, magnesium, potassium, and sodium) for the impinger catch solutions to examine chemical composition of condensable inorganic PM.

Sulfate was the largest fraction of the condensable inorganic $PM_{2.5}$ (averaging around 47%, figure 7), Ammonium accounted for 12%, and Sodium accounted for 4.4%. Chloride, Nitrate, Fluoride, Bromide, Potassium, Calcium, Lithium, and Magnesium were present in small quantities. The remaining portion of the condensable inorganic PM (29%) could not be identified. The large contributions of ammonium and sulfate to the total $PM_{2.5}$ indicate that control of these two species could significantly reduce $PM_{2.5}$ emissions from NGT power plants. SO_2 may be partially converted to residues in methods like SCAQMD 5.1. The large fraction of the gravimetric total represented by sulfate and ammonia could mean that SO_2 control may be the most effective strategy for reducing $PM_{2.5}$ as measured by SCAQMD 5.1. EPA Method 202 attempts to reduce the aqueous effect by reducing the water and SO_2 contact.

The water in the exhaust was also analyzed to determine whether water injected into the system affected PM. Water condensed in the impingers included the injected water, the water formed when natural gas was burned, and a small amount (about 0.1%) of dilution water from the aqueous ammonia. On average, the injected water accounted for 22% of the total water in the combustion products. Anion analysis of the injection water indicated concentrations of sulfate, chloride, and total nitrogen (i.e. nitrites and

nitrates) were 0.099, 0.068, and 0.30 *ppm* respectively. No fluoride, bromide, or phosphate was found.

Total organic carbon (TOC) was measured from the impinger catch solution using a GE Sievers 900 portable TOC analyzer. TOC was obtained by subtracting total inorganic carbon (TIC) from total carbon. TOC averaged 5.4 *ppm* while TIC was much lower, averaging 0.18 *ppm*.

The result from Method 201A/202 showed a similar trend to those from the Method 201A/5.1. Detailed comparisons of the results by the two methods are beyond the scope of this paper. Readers who are interested in this comparison should see the full report to S.C. A.Q.M.D. [15]. Total $PM_{2.5}$ emissions measured using Methods 201A/202 were 20% lower than those measured using Methods 201A/5.1. For both methods, the condensable inorganic fraction was by far the largest fraction of the $PM_{2.5}$.

3.3 Gaseous Emissions

We monitored O_2, CO_2, NO_x and CO in the NGT exhaust (summary data shown in Table 2). Measurements were taken from a stationary point in the stack throughout the $PM_{2.5}$ testing. The data

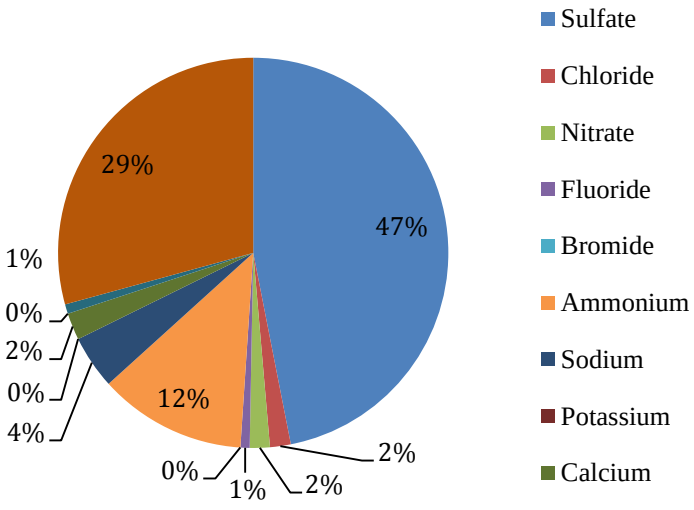

Figure 7: Average Contribution of Ion to Condensable Inorganic PM2.5 Mass Measured Using Method 201A/5.1 from the AAC Laboratory. Note that sulfate makes up the largest portion of ions followed by undetermined and ammonium.

shows that O_2 levels were generally between 13.0% and 13.1%, except during the two test days with the greatest number of turbine load changes on which it increased to 13.3%. As expected, CO_2 levels tracked O_2 levels. NO_x emissions averaged 2.1 *ppmc* (*ppmc* = *ppm*, dry corrected to 15% O_2). CO emissions averaged 1.0 *ppmc*, with daily averages varying from 0.7 to 1.3 *ppmc*.

Table 2: Summary of Gaseous Emissions, Ammonia Slip Measurements, & SO2/SO3 (Daily data can be seen in the supplementary files)

	O_2 % dry	CO_2 % dry	NO_x *ppm* dry	CO *ppm* dry	NO_x *ppm* @ 15% O_2	CO *ppm* @ 15% O_2
Average	13.11	4.44	2.74	1.35	2.07	1.02

	ppm NH_3 (flue gas)	ppm NH_3 @ 15% O_2	Stack O_2 (%)	Std Sample Vol.	Moisture Fraction	SO_2 *ppm* dry	SO_2 *ppm* dry @ 15%O_2	SO_3/SO_x Ratio	SO_3 *ppm* dry @ 15%O_2	SO_3/SO_x Ratio %
Average	4.8	3.5	13.05	223.774	0.107	0.06	0.045	0.017	0.013	22.9

Ammonia (NH_3) slip tests were performed to determine whether the turbine was injecting the correct amount of NH_3 into the SCR unit. Measurements were made at each of the 12 sample points and samples were taken for 5 minutes at each point. NH_3 slip measured in the stack averaged 4.8 *ppm*, or 3.6 *ppmc*, in compliance with permit conditions. NH_3 slip was higher than usual for a new combined cycle SCR system. This was possibly due to a NH_3 slip imbalance entering the catalyst, some flue gas bypassing the catalyst, or low catalyst volume.

SO_x were measured because of their ability to form sulfuric acid in the atmosphere. The SO_x triplicate tests were performed on three days (once per day) with target run times of 8 hours. All of the SO_x were created by the oxidation of sulfur compounds present in the natural gas when it was burned. Measured SO_2 emissions averaged 0.060 *ppm*. When corrected to 15% O_2, SO_2 emissions averaged 0.045 *ppmc*.

Measured SO_3 emissions averaged 0.017 *ppm* at the stack. SO_3 emissions averaged 0.013 *ppmc*. SO_3 accounted for an average of 23% of the total SO_x emissions. While some of the SO_3 was formed in the combustion process, it is likely that more was formed as the SO_2 (a product of combustion) passed across the oxidizing CO and SCR catalysts. If we assume that all of the 0.060 *ppm* SO_x (at STP T=298*K*) measured in the exhaust was converted from sulfur in the fuel then there is about 0.34 *grain/100scf* of sulfur in the fuel, this is within the average range of sulfur concentrations for California pipeline natural gas (0.25-1 *grain/100scf*).

4. Discussion and Conclusion

NGTs currently supply over half of the electricity used in California and this percentage has been increasing due to a decrease of hydroelectric and nuclear power generation. This study furthers our understanding of particle size distributions of NGTs and the nature of particles at different modes.

The NGT exhausted on average $2.3x10^3$ times higher particle number concentrations than ambient air. At the 100 *nm* size, stack particle concentrations were about 20 times higher than ambient air, and increased to $3.9x10^4$ times higher, on average, in the 2.5 *nm* - 3 *nm* particle size range. The ambient air PM mass calculated from the SMPS data was in the range of the AQI PM mass reported that day for the region. Ambient air particle concentrations were slightly higher than average urban Southern California levels due to the test site being located next to a train yard and near a major highway. The loading of $PM_{2.5}$ in the exhaust, measured using Method 201A/5.1,

was within regulatory limits. Of the total $PM_{2.5}$: 8.1% was condensable organic PM, 84.8% was condensable inorganic PM, and 7.1% was solid PM, and PM mass calculated by the SMPS data was within a factor of three compared to the mass reported by Method 201A/5.1.

This study found that the exhaust from the turbine contained higher concentrations of nanoparticles than there were present in ambient air. Further research to determine the nature and volatility of the (sub-10 *nm*) ultrafine particles observed in this study is essential to understand the nature of those particles and their potential harm to human health.

Chapter 2

Reducing Mobile Air Conditioner Power Consumption Using Active Cabin Air Recirculation in Hybrid Electric Vehicles

Eli Brewer[1,2], Heejung S. Jung[1,2]

[1]University of California Riverside (UCR), Department of Mechanical Engineering, Riverside, CA 92521

[2]University of California Riverside, College of Engineering, Center for Environmental Research and Technology (CE-CERT), Riverside, CA 92521

1. Introduction

New government regulations have demanded an increase in automotive fuel economy to reduce dependency on imported oil for transportation [42]. As a result, automotive manufacturers are working to improve the efficiency of powertrains as well as parts of the vehicle that were previously considered adequate in terms of their cost vs benefit. According to the Intergovernmental Panel on Climate Change, emissions of CO_2 are considered the largest anthropogenic radiative force driving climate change [43]. Today, a fraction of a percent of increased mileage is significant, due to its impact on CO_2 emissions. The largest consumer of accessory vehicle power is the Mobile Air Conditioner (MAC). The MAC compressor puts a significant load on the power plant, especially in automobiles with smaller engines but similar cabin size, where the expectation for cooling is the same (to cool up to five passengers in a similar cabin

volume). Smaller power plants have become much more common in hybrid-electric vehicles (HEV). The thermodynamic properties of the refrigeration cycle are inherently inefficient and are ideally designed for heat reservoirs, however, in the automotive industry, both size and weight are limited. Use of the MAC decreases mileage, increases tailpipe CO_2 emissions per mile driven, and can drastically reduce electric vehicle (EV) range. MAC operation can reduce an EV vehicle's fuel economy by up to 35% [44]. Miles per gallon (*mpg*) and in kilowatt-hour per 100 miles (*kWh/100mi*) will both be called fuel economy.

Improving MAC efficiency has become a priority for a number of regulatory agencies. Automotive mileage ratings are now considering MAC consumption in the SC03 and AC17 Federal Test Procedures (FTP) while the standard FTP cycle does not account for any accessory use [45]. Two significant improvements made by automotive manufacturers are: 1. A thermostat controlled HVAC system that allows the passengers to set the desired cabin temperature (theoretically preventing over-cooling), and 2. An electric, variable compressor that allows for and adjusts partial load, which reduces the MAC power, once the desired temperature is reached.

Southern California and the majority the Pacific Southwest Region are typically hot, dry, and sunny, leading to heavier MAC use. California as a whole uses the MAC 13% of the time. However, this value is skewed low because the study was conducted primarily in coastal California cities, which are significantly cooler than inland communities [46]. Additionally, a more recent report found California drivers use the

MAC 29% of the time [47]. Drivers in Nevada use the MAC 38% of the time, Arizona 54% of the time, and Hawaii 70% of the time [46].

A cabin air recirculation system was proposed by Grady and Jung [27] to improve cabin air quality by reducing the pollutant particle concentrations. Cabin air recirculation reduces the total air mass cooled by the MAC, which can reduce the MAC energy consumption and improve vehicle mileage. The compressor in older MACs works at a fixed power setting regardless of the cabin air temperature, whereas a cabin air temperature sensor modulates the compressor power in newer MACs. A modern MAC has a significant advantage over older MACs due to the new electric compressors that are capable of operating at a range of loads, as opposed to the traditional on-off operation. The goal of this study was to evaluate the impact of cabin air recirculation on the efficiency of the MAC. The experiments were designed to closely investigate the operation of the AC automatic cooling mode (specifically the direct impact of cabin air recirculation) and quantify its impact on fuel economy in Hybrid-Electric Vehicles. The study also presents the additional benefit of cleaner cabin air, in terms of particle concentrations, from cabin air recirculation.

2. Experimental

2.1 Instruments

The primary instrument used to monitor the vehicle's status was an On Board Diagnostic (OBDII) Pro ScanTool that queries 16 different parameters per second. The OBDII ScanTool is operated by a laptop that records the data using the Mobile Energy

Emission Telenetics System (M.E.E.T.S.) software [48]. UC Riverside's College of Engineering Center for Environmental Research and Technology (CE-CERT) developed this software. The current version of the software was optimized to reduce load on the computer CPU and increase battery life. Parameter Identifications (PIDs) were queried and recorded at roughly 0.53 Hz. All of the on-road data was taken while the vehicle was in EV (Electric Vehicle) mode, so the primary battery of the hybrid vehicle supplied all of the power. For these tests, several SAE Standard J1979 defined PIDs were used along with several Toyota defined PIDs (Appendix A). The primary parameters monitored were the voltages of the battery block, the battery amperage, vehicle speed, state of charge (SOC) of the battery, and AC power. Other studies have shown that OBDII PIDs can effectively measure fuel economy [49].

We also used two thermocouples (Omega OM-EL-USB) to record in-cabin, and outside air temperatures during the test. The in-cabin thermocouple was mounted 6 inches above the middle of the armrest between the driver and passenger seats, and the outside thermocouple's lead wire was routed an inch outside the rear, right passenger door.

A CO_2 concentration analyzer (CIRAS SC), and an aerosol diameter concentration analyzer (TSI EAD 3070A) were used in-cabin on a series of highway tests. These instruments give a quantitative measure of in-cabin air quality. The CIRAS SC is an infrared CO_2 sensor capable of measuring CO_2 in the range of 0-9,999 *ppm.* CO_2 in the cabin above the ambient level (~440 *ppm*) generally comes from the occupant's respiration, and the O.S.H.A. 8 hour maximum is a 5,000 ppm time weighted average.

The electrical aerosol detector (EAD) uses a corona discharge needle to charge particles, and an electrometer to detect aerosol diameter concentration. The EAD measures aerosol diameter concentration providing a measure of the surface area deposition in the lung and the depth to which the particles are penetrating into the lungs [25]. Mortality rates have been shown increase among groups with long-term exposure to fine and ultrafine particles [50].

2.2 Vehicles

The primary vehicle used in this study, was a 2012 Toyota Prius Plug-in, however, a 2012 Nissan Leaf was used for several tests for comparison. The 2012 Prius Plug-in has two power plants: a 1.8 *L* I-4 98hp gasoline Atkinson cycle engine, producing 105 *lb-ft* torque, and an electric 80 *hp*/60 *kW* permanent magnet AC synchronous motor, producing 153 *lb-ft* torque. Together, these two to produce 134 hp with a combined fuel economy of 49 *MPG* [51]. Additionally, the Prius Plug-in has a 4.4 *kWh* lithium-ion battery.

The Prius Plug-in was chosen as the primary vehicle for this study because the Prius series were the top selling hybrid vehicles in the U.S. market at the time, and the Plug-in model uniquely spanned both Hybrid Vehicle (HV) technologies and Electric Vehicle (EV) technologies with its 12 mile EV range. The Prius has been shown to perform more efficiently than other similar vehicles due to its Atkinson cycle engine, and its electrical scroll compressor [52]. The Atkinson cycle engine is more efficient due to its unconventional valve timings and greater expansion ratio [53].

Table 3: Toyota Prius Plug-in and Nissan Leaf selected Specifications

	2012 Toyota Prius Plug-in	*2012 Nissan Leaf*
Total hp	*80*	*110*
Battery Size kWh	*4.4*	*24*
All-Electric Range km (mi)	*18.8 (11.7)*	*117 (73)*
Curb Weight kg (lb)	*1,436 (3,165)*	*1,521 (3,354)*
Electric Motor size kW	*60*	*80*
Torque lb-ft	*153*	*187*
Fuel Economy MPGe	*95*	*99*
Fuel Economy kWh/100 mi	*29*	*34*

2.3 Tests

This study varied AC recirculation and outside temperature. AC recirculation was varied in four modes: AC Off (ACO), AC on Recirculated air (ACR), AC on Partial (ACP), and AC on Fresh air (ACF). In ACO mode, the AC and blower were turned off. In ACR mode the AC was put on the automatic thermostat setting, with the temperature set to 72 °*F*, and the air set to recirculate. In ACP the AC was put on the automatic thermostat setting, with the temperature set to 72 °*F*, the air set to fresh, and the recirculation door was manually adjusted to allow ~20% recirculated air. In ACF the AC was put on the automatic thermostat setting, with the temperature set to 72 °*F*, and the air set to fresh.

2.3.1 On-Road Test Route

The test route (shown in figure 8) was chosen because it was near the CE-CERT facility, the length was similar to that of the Federal Test Procedure SC03 route used in

the lab later in this study [54], and the drive was highly repeatable due to the low traffic volume and lack of signal lights. The high repeatability can be seen in the average speeds of the on-road tests are shown in figure 9. Real-world driving presents the challenge of uncontrollable variables, particularly in the form of the random nature of other drivers. This often causes on-road data to be considerably different from lab data. Therefore, it was important to compare our lab tests with real on-road tests. Variations in the on-road tests are to be expected, however, this route was highly repeatable and several steps were taken to reduce error. A single driver completed all trips, testing was performed in sets of three consecutive trips (each with one of the three main AC modes), and the order of AC conditions were shuffled to eliminate order bias.

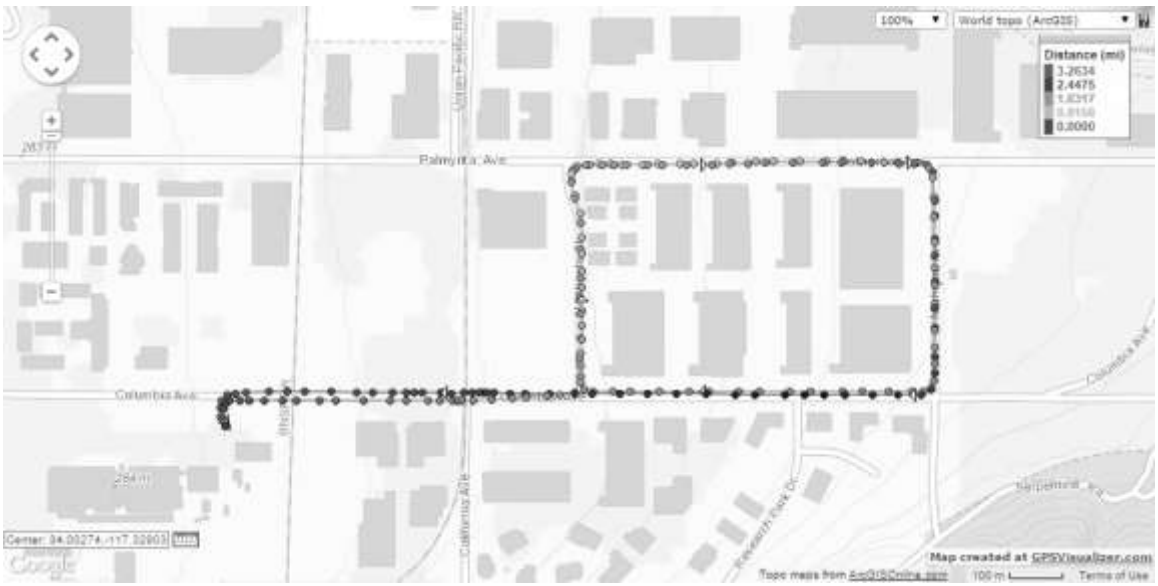

Figure 8: On-Road Charge Depletion Route 3.34 Miles. Map created with GPSVisualizer.com using ArcGIS World topo [59]

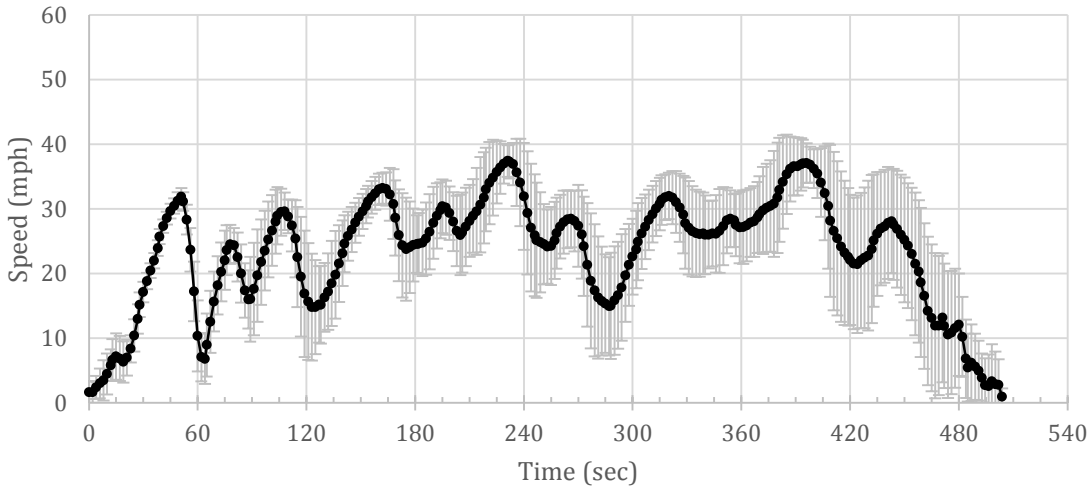

Figure 9: Average Speed Plot On-Road Route. The relatively low variability of the speed indicates that our testing was highly repeatable.

2.3.2 Laboratory Test SC03

Supplemental Federal Test Procedure (SFTP) SC03 (figure 10) is a U.S. EPA driving cycle. We conducted SC03 tests using a chassis dynamometer at UC Riverside's

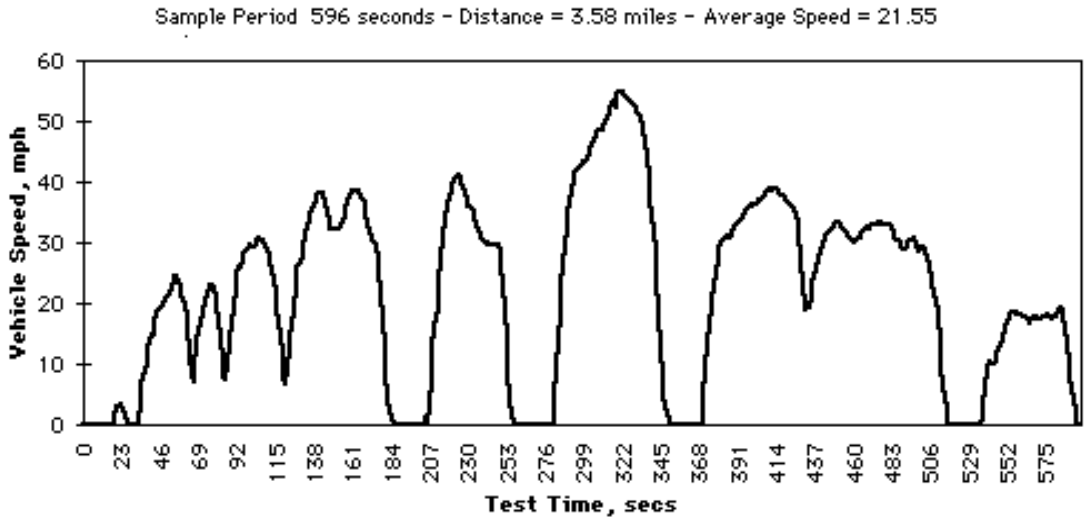

Figure 10: FTP SC03 driving cycle speed plot used for in-lab chassis testing of the Prius. It is designed to simulate the rapid braking and accelerations that are seen in real-world driving. It also utilizes the air conditioner. [54]

Vehicle Emission Research Laboratory (VERL) located at the CE-CERT facility. VERL uses a Pierburg AMA-2000 Exhaust Emissions Measuring System to measure CO_2 and other regulated vehicle emissions. The SC03 driving cycle has quick accelerations and decelerations, and requires use of the vehicle's air conditioner, which was designed to give it characteristics similar to that of real-world driving.

The Federal Test Procedures give detailed descriptions of all test conditions and methods [55]. For our tests, the Prius' windows were closed, the automatic air conditioning thermostat was set to 72 °F, and the recirculation flap was set either to full air recirculate to full fresh. The vehicle sat inside the lab overnight, prior to testing, and was preconditioned by driving at 50 mph for 20 minutes prior to the three SC03 driving cycles on the dynamometer (figure 11). The first set of three SC03 driving cycles began immediately after preconditioning. Each set of three SC03 driving cycles featured a

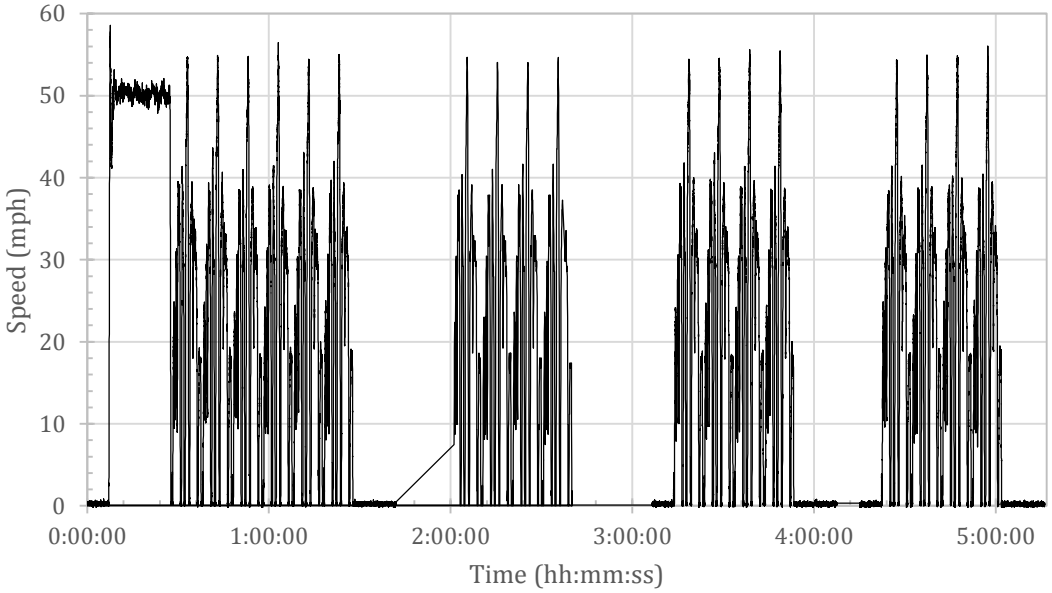

Figure 11: Example speed plot from day 2 of testing. Each peak is the middle of a single SC03 test.

shuffled sequence of ACO, ACR, and ACF (figure 12). Following the three SC03 driving cycles was a 30-minute break after which a single SC03 driving cycle was used to warm the car back up. Another set of three back-to-back SC03 driving cycles immediately followed the warm-up. While VERL meets the minimum test cell size, and uses the appropriate cooling fan it is not a climate-controlled facility. To approximate the required ambient temperature and humidity (35.0 ± 3.0 °C, and 100 grains of water per pound of dry air, or 27.4 RH%) we manually controlled the ventilation of AC system to maintain a temperature of 33.7 °C with a σ of 0.9 °C. Humidity could not be controlled, but was on average 51.3 RH% with a σ of 7.8 RH%. VERL does not have any form of simulated solar heating lamp, and SC03 requires a solar load of 850 ± 45 W/m^2, therefore we were unable to meet this specification.

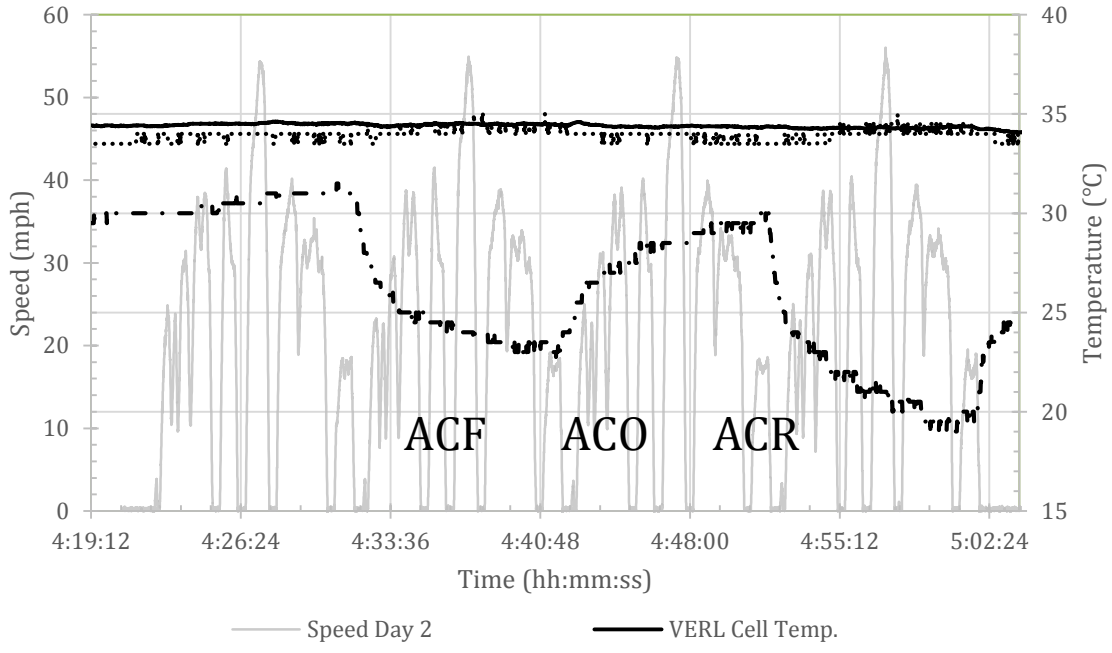

Figure 12: Example of best controlled in-lab temperature for set of three SC03 driving cycle tests. ACO heats cabin back up to within 1 °C of pre-ACF test.

The SC03 tests were performed with the Prius in Charge Sustaining (CS) mode because the harsh accelerations caused the on board computer to engage the gasoline engine and we were interested in hybrid fuel economy data. The test cycle represents a 3.6 *mile* (5.8 *km*) route with an average speed of 21.6 *mph* (34.8 *kph*), maximum speed 54.8 *mph* (88.2 *kph*), and duration of 596 *sec*. The SC03 cycle was repeated three times with each AC condition.

2.3.3 Highway

Six highway tests were performed along the 91 Freeway, during rush hours, from CE-CERT to Gypsum Canyon Road and back (52 *miles*) to measure in-cabin air quality in high traffic conditions. AC modes were the same as the previous on-road conditions with a repeated test for ACR and ACF, one test of ACO and ACP. We measured in-cabin CO_2 and aerosol diameter concentration. Every 20-30 *min*. the cabin air was cycled with ambient air from the outside to test the repeatability of the AC mode to remove particles.

2.4 Calculating Fuel Economy

Fuel Economy was calculated by the following equations:

$$Fuel\ Economy = (P_e + P_g)/distance * 100 \qquad \textit{Equation 2}$$

Where P_e is the electric power, and P_g gasoline power in final units of *kWh/100mi*. Electric power was obtained from integrating over the values of battery current and voltage measured by the OBD-II. Gasoline power is derived from instantaneous

measurements of Mass Air Flow (MAF) through the engine (also from the OBD-II). The power from gasoline can be found as follows:

$$P_g = \frac{MAF*44.4}{14.7} * .333 \qquad \textit{Equation 3}$$

Where it is assumed that the on-board computer maintains the fuel to air ratio at an ideal stoichiometric ratio ($\frac{14.7\ g\ O_2}{g\ C_8H_{18}}$), the mass energy density (or energy content) of gasoline is 44.4 MJ/kg, and the standard efficiency for the internal combustion engine is 33.3%.

Fuel Economy was also calculated (Equation 6) from tail pipe emissions captured by VERL. The carbon balance method used is described in CFR, Title 40, Part 86 [56]. This method assumes that the mass of the carbon atom in the exhaust is equal to the amount of carbon burned in the fuel.

$$Fuel\ Economy\,(Carbon\ Balance) = \frac{(CWF \cdot SG \cdot 3781.8)}{(0.866 \cdot THC + 0.429 \cdot CO + 0.273 \cdot CO_2)} \qquad \textit{Equation 4}$$

Where 3781.8 is the density of water at 60 °*F* in *g/gal*, THC is the Total Hydrocarbon emission rate in *g/mile*, CO is the emission rate of Carbon Monoxide in *g/mile* and CO_2 is emission rate of Carbon Dioxide in *g/mile*, CWF is the Carbon Weight Fraction of the test fuel, and SG is the specific gravity of the test fuel [57]. The exhaust gas is captured in a sample bag throughout the SC03 cycle and then the concentration of carbon containing gas is measured.

3. Results

3.1 SC03 Driving Cycles

The OBD fuel economy data is highly reliable based on a direct comparison and linear regression with the carbon balance method fuel economy data (figure 13). MAC energy consumption depends heavily on the ambient temperature outside the vehicle. The difference is easily apparent for the SC03 driving cycles (figure 14). This is due to the fact that the SC03 is designed to simulate real-world driving conditions with AC use and magnifies differences in fuel economy. The Prius' AC consumed an average of 34.16% of all power with a σ of 2.54% when the MAC was set to fresh air, whereas it consumed an average 29.26% of all power with a σ of 3.98% when the AC was set to recirculated air. The AC energy consumption reported shows distinct trends of increased energy consumption with increased ambient temperature (figure 14). The Prius averaged 38.11 *kWh/100mi* when the AC was set to fresh air, 32.98 *kWh/100mi* with recirculated air, and 24.52 *kWh/100mi* with the AC off. Three data sets were removed from the in-lab SC03 data due to instrument error where there are significant gaps in the data (one from ACF and two from ACR).An additional test from each AC test mode was removed due to

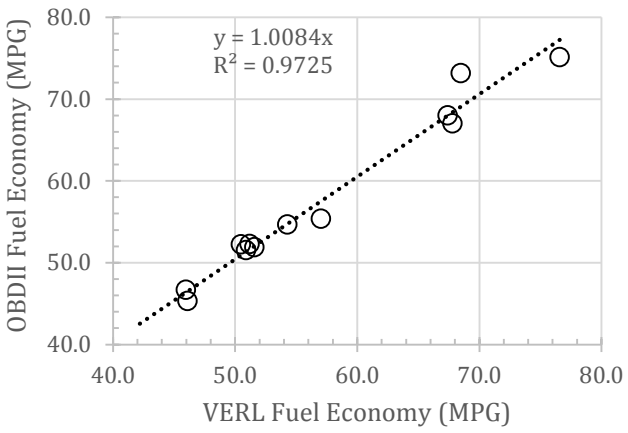

Figure 13: VERL vs. OBDII fuel economy. Highly reliable OBDII data shows that the OBDII data is an appropriate tool for measuring fuel economy.

the Prius underutilizing the battery, which was apparent from the electric power behavior (these tests did not charge the battery during heavier braking).

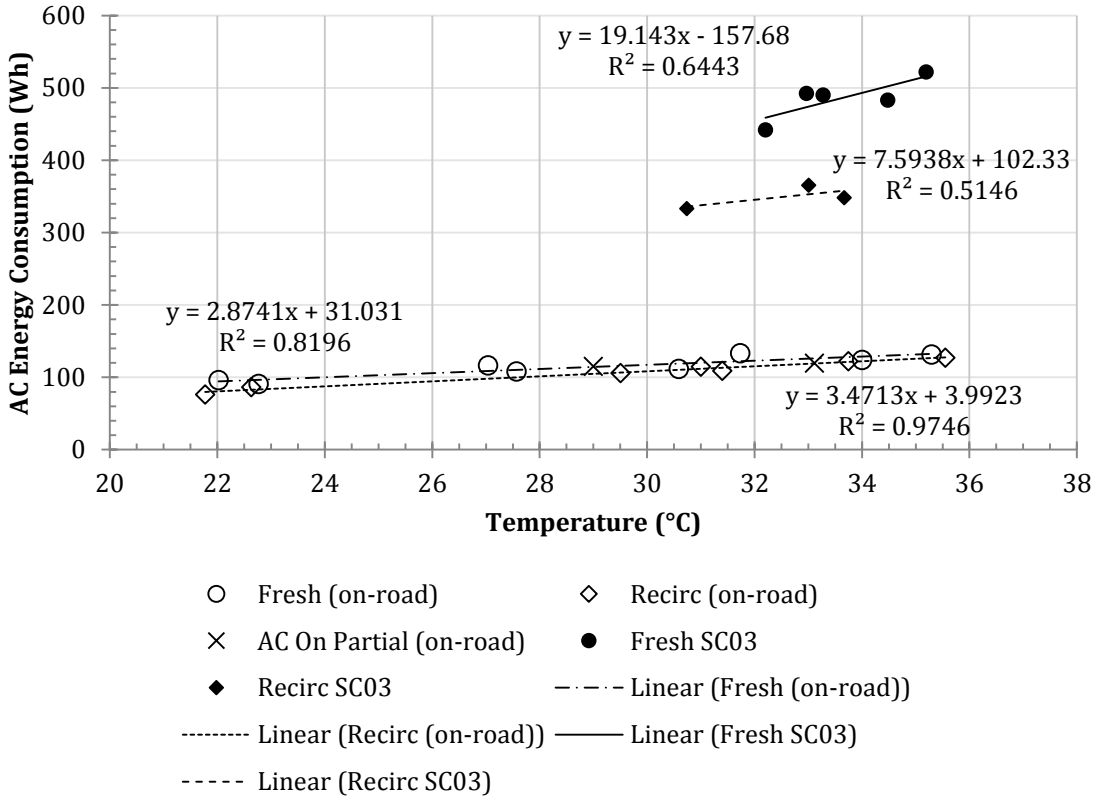

Figure 14: AC Energy consumption. All data shows increasing trend with temperature as is expected for the MAC to cool the cabin more. On-road data reduced consumption likely implemented by Toyota to improve EV range.

3.2 On-Road

The vehicle mileage (obtained from OBD-II) increases with the ambient air temperatures (figure 15) for both the Prius and the Leaf. The Prius averaged 28.44 *kWh/100mi* on-road when the AC was set to fresh air, 26.71 *kWh/100mi* with the AC set to recirculated air, and 20.53 *kWh/100mi* with the AC was off. The MAC energy

consumption (figure 14) does not show a great distinction between AC modes during the on-road test, however in-lab testing showed a significant separation between ACR and ACF. Despite the small differences in the AC energy consumption, the fuel economy of the ACR and ACF conditions are significantly different when normalized by the average ACO fuel economy (figure 16). Both on-road and in-lab data display an increasing trend of fuel consumption with temperature, and significant differences between ACF and ACR; fresh air uses about 8% more fuel than AC on recirculated air (normalized by the AC off case) for the on-road tests and about 20% more for the in-lab tests.

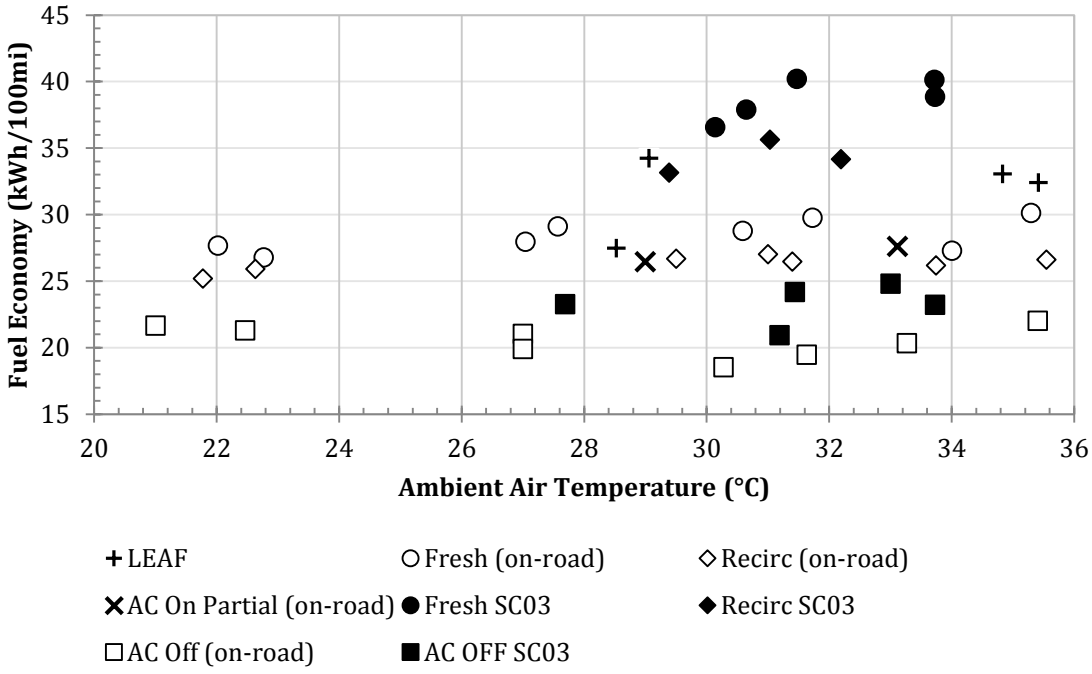

Figure 15: Fuel Economy from all tests calculated from the OBDII. Separation of on-road and in-lab data indicated how the Prius operates differently under different driving modes. The Leaf fuel economy is in the range of the Prius' fuel economy.

3.3 In-Cabin Air Quality

Cabin air recirculation reduced the particle diameter concentration by more than a factor of ten when compared to fresh air (figure 17). Cabin air recirculation also increased the concentration of CO_2 in the cabin air at a constant rate (~500 *ppm* every 4 *min.*) at low speeds, however 1 *min.* of fresh air reduced CO_2 concentrations by a factor of ten, equal to that of ambient air. Cabin air recirculation also reduced particle concentrations by a factor of ten and acted as a buffer against high concentrations of particles in ambient air on the highway. ACF shifted the mean particle diameter concentration from the ambient concentration of 1.7 mm/cm^3 to 0.6 mm/cm^3, and ACR further dropped the concentration to about 0.15 mm/cm^3 (figure 18).

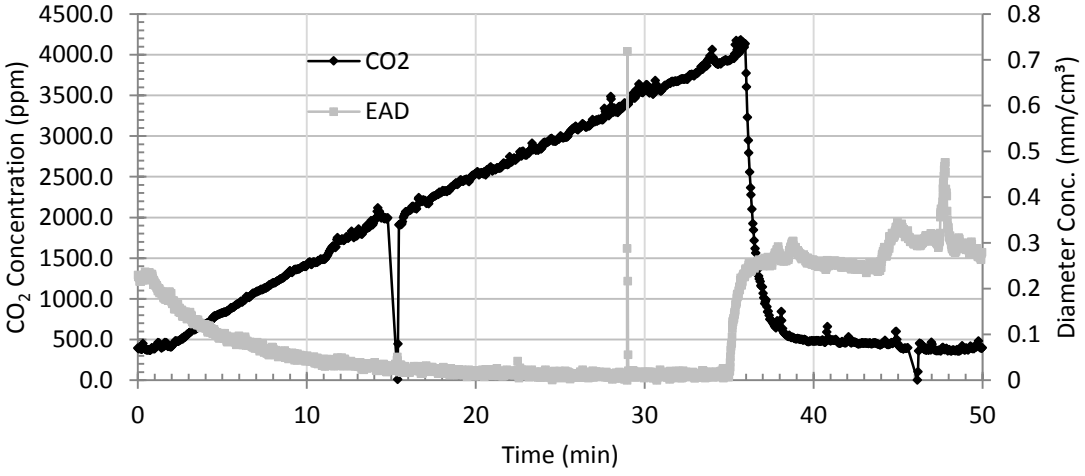

Figure 16: CO_2 Clear Test from recirculate to fresh air. Ambient CO2 concentration levels were achieved within 1 minute of switching from recirculate to fresh air.

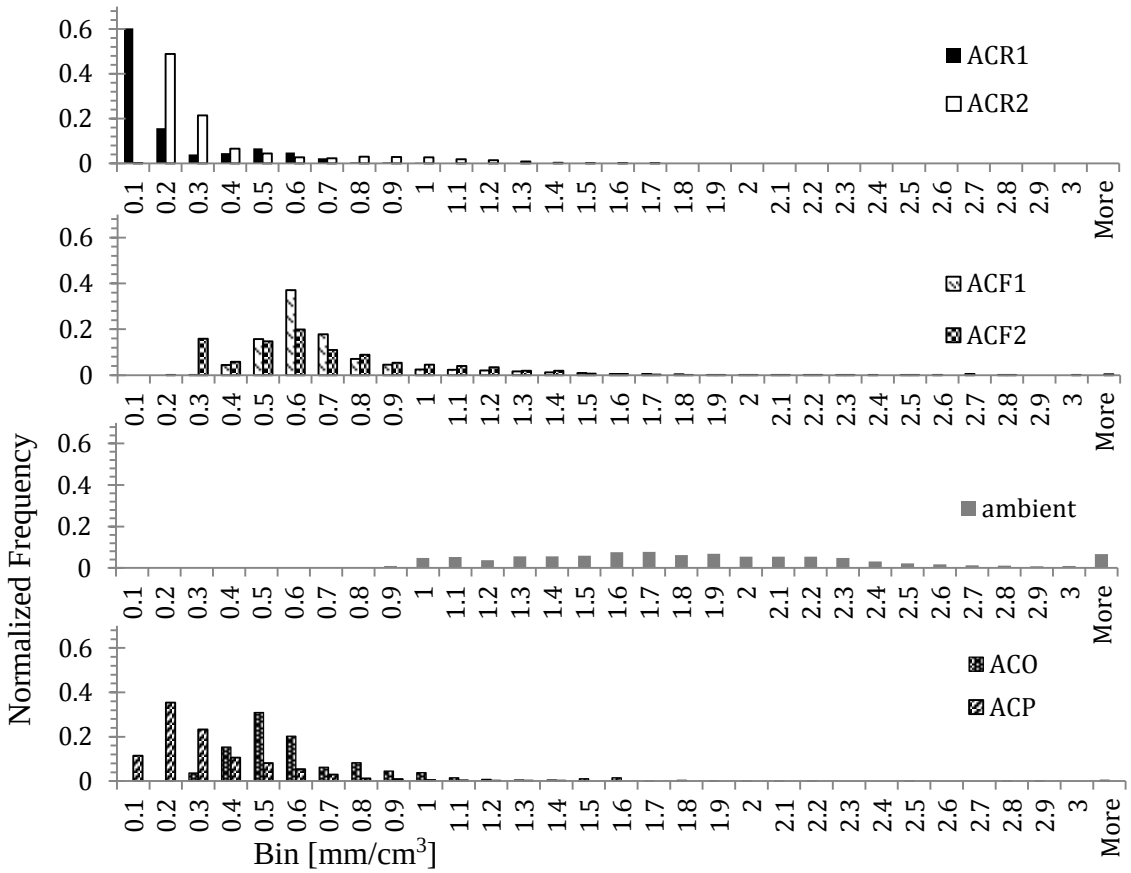

Figure 17: Normalized histograms of highway EAD data. ACR reduces particle concentrations in the vehicle cabin. In-cabin air quality is significantly improved by the reduction of particles, while CO2 increases tenfold after 35 min., particles reduce tenfold after only 16 min. Ambient data is from a similar trip on the 91 fwy. in July by Liem Pham.

4. Conclusions

Overall, this study has found that MAC energy consumption and vehicle mileage can be accurately obtained by recording OBD II parameters, and that this method and device are appropriate tools for the evaluation of MAC energy consumption in hybrid and plug-in hybrid vehicles. It is beneficial for the user to operate a vehicle with the AC set to recirculate as it saves fuel, extends the vehicle's range, and reduces PM in the cabin.

The on-road and lab tests are not identical, however they both have very similar trends that lead us to the same conclusions. The Prius consumed 8% more power when the MAC was set to fresh air than when the MAC was set to recirculated air. The MAC energy consumption varied significantly depending on the driving cycle. The MAC energy consumption ranged from 8% to 12% (percent of total energy consumed per trip) for the on-road driving route used in this study, and the MAC energy consumption ranged from 22% to 38% for the in-lab test using the SC03 driving cycle. Fuel economy is significantly improved by using AC on recirculate in all tests. Additionally, in-cabin air quality is significantly improved by the reduction of particles, while CO_2 increases tenfold after 35 minutes, particles reduce tenfold after only 16 min. Overall, improvements in air quality can be easily made without endangering the passengers with high levels of CO_2.

References:

[1] (EIA), US Energy Information Administration, 2013, "Updated Capital Cost Estimates for Utility Scale Electricity Generating Plants," (April).

[2] Southern California Edison, 2013, "Southern California Edison Announces Plans to Retire San Onofre Nuclear Generating Station," pp. 1–3.

[3] California Energy Commission C., 2014, "California Electrical Energy Generation* Total Production, by Resource Type (Gigawatt Hours)" [Online]. Available: http://www.energyalmanac.ca.gov/electricity/electricity_generation.html. [Accessed: 07-Aug-2014].

[4] (EIA) U. E. I. A., 2013, "U.S. Natural Gas Prices" [Online]. Available: http://www.eia.gov/dnav/ng/ng_pri_sum_dcu_nus_m.htm. [Accessed: 06-Nov-2013].

[5] (EIA) U. E. I. A., 2013, Annual Energy Outlook 2013, US Departrment of Energy, Washington, D.C.

[6] England G. C., Watson J. G., Chow J. C., Zielinska B., Chang M., Loos K. R., and Hidy G. M., 2007, "Dilution-Based Emissions Sampling from Stationary Sources: Part 1- Compact Sampler Methodology and Performance," J. Air Waste Manage. Assoc., **57**(1), pp. 65–78.

[7] Tamura T., and Tetra Tech, 2013, GAP ANALYSIS FOR THE STATIONARY COMBUSTION FILTERABLE AND CONDENSABLE PARTICULATE MATTER EMISSION FACTORS.

[8] Klippel N., Kasper M., and Bengtsson K., 2002, "Gas Turbines – Sources or Sinks for Ambient Air Aerosols ?," (August), pp. 1–11.

[9] Mohr M., Ylätalo S., Riccius O., and Kauppinen E., 1995, "Formation of ultrafine particles inside an electrostatic precipitator caused by interaction of denitrification unit and corona discharge," J. Aerosol Sci., **26**, pp. 871–872.

[10] Schmatloch V., 2000, "4th ETH Conference on Nanoparticle Measurement."

[11] SOUTH COAST AIR QUALITY MANAGEMENT DISTRICT S., 2002, RULE 1303.

[12] Elder A., and Oberdörster G., 2005, "Translocation and Effects of Ultrafine Particles Outside of the Lung," Clin. Occup. Environ. Med., **5**(4), pp. 785–796.

[13] Health Effects Institute, 2013, "Understanding the Health Effects of Ambient Ultrafine Particles," (January), p. 122.

[14] FERCo, UC Irvine, UC Riverside, Environ Co., and Allied Environmental Technologies, 2009, CONTROL STRATEGIES AND TECHNOLOGIES FOR PARTICULATE MATTER UNDER 2.5 MICRONS (PM2.5) AND ULTRA FINE PARTICULATE EMISSIONS FROM NATURAL GAS-FIRED TURBINE POWER PLANTS: PHASE 1 – TECHNICAL ASSESSMENT.

[15] FERCo, Delta, and UC Riverside, 2014, CONTROL STRATEGIES AND TECHNOLOGIES FOR PARTICULATE MATTER UNDER 2.5 MICRONS (PM2.5) AND ULTRA FINE PARTICULATE EMISSIONS FROM NATURAL GAS-FIRED TURBINE POWER PLANTS: PHASE 2 – GE LMS100 TEST RESULTS.

[16] 1989, METHOD 5.1 DETERMINATION OF PARTICULATE MATTER EMISSIONS FROM STATIONARY SOURCES USING A WET IMPINGEMENT TRAIN.

[17] 2010, Method 201A—Determination of PM10 and PM2.5 Emissions From Stationary Sources (Constant Sampling Rate Procedure), 40 C.F.R. pt. 51 Appendix M.

[18] General Electric Water and Power, 2013, "GE Aeroderivative Product and Services Solutions."

[19] California Energy Commission C., 2008, ENERGY COMMISSION WALNUT CREEK DECISION CALIFORNIA.

[20] Abdul-Khalek I., 1996, "Online measurement of volatile and solid exhaust particles using a catalytic stripper system : characterization and application," Thesis (M.S.)--University of Minnesota, 1996.

[21] Murphy S. M., Agrawal H., Sorooshian A., Padró L. T., Gates H., Hersey S., Welch W. a, Lung H., Miller J. W., Cocker D. R., Nenes A., Jonsson H. H., Flagan R. C., and Seinfeld J. H., 2009, "Comprehensive simultaneous shipboard and airborne characterization of exhaust from a modern container ship at sea.," Environ. Sci. Technol., **43**(13), pp. 4626–40.

[22] Abdul-Khalek I. S., and Kittelson D. B., 1995, Real Time Measurement of Volatile and Solid Exhaust Particles Using a Catalytic Stripper.

[23] Stenitzer M., 2003, Nano particle formation in the exhaust of internal combustion engines, na.

[24] TSI, 2012, "ELECTRICAL AEROSOL DETECTOR MODEL 3070A."

[25] Wilson W. E., Stanek J., Han H.-S. (Ryan), Johnson T., Sakurai H., Pui D. Y. H., And J. T., Chen D.-R., and Duthie S., 2007, "Use of the Electrical Aerosol Detector as an Indicator of the Surface Area of Fine Particles Deposited in the Lung," J. Air Waste Manage. Assoc., **57**(2), pp. 211–220.

[26] Nguyen A., and Jung H., 2014, "Influence of Wind and Driving Conditions on Self-Polluting Tailpipe Emission [In Preparation]."

[27] Grady M. L., Jung H., Kim Y. C., Park J. K., and Lee B. C., 2013, Vehicle Cabin Air Quality with Fractional Air Recirculation.

[28] Zhu Y., Eiguren-Fernandez A., Hinds W. C., and Miguel A. H., 2007, "In-cabin commuter exposure to ultrafine particles on Los Angeles freeways.," Environ. Sci. Technol., **41**, pp. 2138–2145.

[29] Klippel N., Wood T., Pearce B., Bengtsson K., Kasper M., and Mosimann T., 2004, On-Line Measurement of Ultrafine Particle Emissions from Gas Turbines, Technical report ALSTOM Power.

[30] N. Gysel, Wiliiam A. Welch, Chia-Li Chen, W. Miller D. C., "Development of New PM Test Protocol and Characterization of PM Formation and Growth from Natural Gas Turbines.," Prep.

[31] Lobo P., Hagen D. E., and Whitefield P. D., 2011, "Comparison of PM emissions from a commercial jet engine burning conventional, biomass, and Fischer–Tropsch fuels," Environ. Sci. Technol., **45**(24), pp. 10744–10749.

[32] Herndon S. C., Jayne J. T., Lobo P., Onasch T. B., Fleming G., Hagen D. E., Whitefield P. D., and Miake-Lye R. C., 2008, "Commercial aircraft engine emissions characterization of in-use aircraft at Hartsfield-Jackson Atlanta International Airport.," Environ. Sci. Technol., **42**(6), pp. 1877–83.

[33] England G. C., Thomas P. McGrath, and GE Energy and Environmental Research Corporation, 2004, Development of Fine Particulate Emission Factors and Speciation Profiles for Oil and Gas-fired Combustion Systems, TOPICAL REPORT: TEST RESULTS FOR A COGENERATION PLANT WITH SUPPLEMENTARY FIRING, OXIDATION CATALYST AND SCR AT SITE GOLF.

[34] Chang M. C. O., and England G. C., 2004, "Development of Fine Particulate Emission Factors and Speciation Profiles for Oil and Gas-Fired Combustion Systems, Other Report: Pilot Scale Dilution Sampler Design and Validation Tests (Laboratory Study)," (DOE Contract No. DE-FC26-00BC15327,nGRI contract No. 8362\nAPI Contract No. 00-0000-4303,), p. 130.

[35] Wien S., Glenn C. England, Chang M., and GE Energy and Environmental Research Corporation, 2004, Development of Fine Particulate Emission Factors and Speciation Profiles for Oil and Gas-fired Combustion Systems, TOPICAL REPORT: TEST RESULTS FOR A COMBINED CYCLE POWER PLANT WITH SUPPLEMENTARY FIRING, OXIDATION CATALYST AND SCR AT SITE BRAVO.

[36] England G. C., Wien S., McGrath T. P., Hernandez D., and GE Energy and Environmental Research Corporation, 2004, Development of Fine Particulate Emission Factors and Speciation Profiles for Oil and Gas-fired Combustion Systems, TOPICAL REPORT: TEST RESULTS FOR A COMBINED CYCLE POWER PLANT WITH OXIDATION CATALYST AND SCR AT SITE ECHO.

[37] Buseck P. R., and Adachi K., 2008, "Nanoparticles in the Atmosphere," Elements, **4**(6), pp. 389–394.

[38] Kuwata M., Zorn S. R., and Martin S. T., 2012, "Using elemental ratios to predict the density of organic material composed of carbon, hydrogen, and oxygen.," Environ. Sci. Technol., **46**(2), pp. 787–94.

[39] Nakao S., Tang P., Tang X., Clark C. H., Qi L., Seo E., Asa-Awuku A., and Cocker D., 2013, "Density and elemental ratios of secondary organic aerosol: Application of a density prediction method," Atmos. Environ., **68**, pp. 273–277.

[40] Maricq M. M., and Xu N., 2004, "The effective density and fractal dimension of soot particles from premixed flames and motor vehicle exhaust," J. Aerosol Sci., **35**, pp. 1251–1274.

[41] Zheng Z., Durbin T. D., Karavalakis G., Johnson K. C., Chaudhary A., Cocker D. R., Herner J. D., Robertson W. H., Huai T., Ayala A., Kittelson D. B., and Jung H. S., 2012, "Nature of Sub-23-nm Particles Downstream of the European Particle Measurement Programme (PMP)-Compliant System: A Real-Time Data Perspective," Aerosol Sci. Technol., **46**(8), pp. 886–896.

[42] Environmental Protection Agency, 2012, "2017 and later model year light-duty vehicle greenhouse gas emissions and corporate average fuel economy standards; final rule," Fed. Regist., **77**(199).

[43] Lisa Alexander (Australia), Simon Allen (Switzerland/New Zealand), Nathaniel Bindoff (Australia), Francois-Marie Breon (France), John Church (Australia), Ulrich Cubasch (Germany), Seita Emori (Japan), Piers Forster (UK), Pierre Friedlingstein (UK/Belgium) S.-P. X. (USA), 2013, Climate Change 2013 - The Physical Science Basis: Working Group I Contribution to the Fourth Assessment Report of the IPCC.

[44] Bharathan D., Chaney L., Farrington R. B., Lustbader J., Keyser M., and Rugh J., 2007, "An Overview of Vehicle Test and Analysis from NREL ' s A / C Fuel Use Reduction Research," (June).

[45] Sciance F., Nelson B., Yassine M., Patti A., and Rao L., 2013, Developing the AC17 Efficiency Test for Mobile Air Conditioners.

[46] Johnson V. H., 2002, "Fuel Used for Vehicle Air Conditioning: A State-by-State Thermal Comfort-Based Approach."

[47] Rugh J. P., Hovland V., and Andersen S. O., 2004, Significant Fuel Savings and Emission Reductions by Improving Vehicle Air Conditioning.

[48] Menke J., and Scora G., 2011, "Mobile Energy Emission Telenetics System (M.E.E.T.S.)."

[49] DeFries T. H., Sabisch M., Kishan S., Posada F., German J., and Bandivadekar A., 2014, "In-Use Fuel Economy and CO 2 Emissions Measurement using OBD Data on US Light-Duty Vehicles."

[50] Ostro B., Hu J., Goldberg D., Reynolds P., Hertz A., Bernstein L., and Kleeman M. J., 2015, "Associations of Mortality with Long-Term Exposures to Fine and Ultrafine Particles, Species and Sources: Results from the California Teachers Study Cohort," Environ. Health Perspect.

[51] Toyota, 2012, "2012 Prius Plug-in Hybrid Product Information," pp. 1–6.

[52] Khoury G. El, and Clodic D., 2005, Method of Test and Measurements of Fuel Consumption Due to Air Conditioning Operation on the New Prius II Hybrid Vehicle.

[53] Boggs D. L., Hilbert H. S., and Schechter M. M., 1995, The Otto-Atkinson Cycle Engine-Fuel Economy and Emissions Results and Hardware Design.

[54] Environmental Protection Agency, 2013, "Dynamometer Drive Schedules" [Online]. Available: http://www.epa.gov/nvfel/testing/dynamometer.htm.

[55] United States Environmental Protection Agency, 2010, Code of Federal Regulations 40 CFR Part 86, Subpart B—Emission Regulations for 1977 and Later Model Year New Light-Duty Vehicles and New Light-Duty Trucks and New Otto-Cycle Complete Heavy-Duty Vehicles; Test Procedures.

[56] Agency E. P., 2010, "Control of Emissions from New and In-Use Highway Vehicles and Engines (Continued)," **40**.

[57] Durbin T. D., Karavalakis G., Russell R. L., Short D., Hajbabaei M., and Villela M., 2013, API Aromatics Final Report_2013_09.

[58] Usbseawolf2000, 2013, "Prius PHV: Custom PIDs for Torque Android App."

[59] Schneider A., 2015, "GPS Visualizer: Google Maps ArcGIS World topo" [Online]. Available: http://www.gpsvisualizer.com/map?output_google. [Accessed: 08-Jun-2015].

Appendix A: Parameter Identifiers used to query the OBD-II

Table 4: List of On Board Diagnostic Parameter IDs (PID) used in testing. Mode 21 signifies a Toyota defined PID. Letters represent the location of the value in OBD-II output [58]

Mode	PID	Data bytes returned	Description	Units	Formula
21	81	18	Battery Block Voltage -V01	V	(A*256+B)*79.99/65535
21	81	18	Battery Block Voltage -V02	V	(C*256+D)*79.99/65535
21	81	18	Battery Block Voltage -V03	V	(E*256+F)*79.99/65535
21	81	18	Battery Block Voltage -V04	V	(G*256+H)*79.99/65535
21	81	18	Battery Block Voltage -V05	V	(I*256+J)*79.99/65535
21	81	18	Battery Block Voltage -V06	V	(K*256+L)*79.99/65535
21	81	18	Battery Block Voltage -V07	V	(M*256+N)*79.99/65535
21	81	18	Battery Block Voltage -V08	V	(O*256+P)*79.99/65535
01	0C	2	Engine RPM	rpm	((A*256)+B)/4
21	7D	3	AC Power	HP	C*50*0.001341022089595
21	98	9	Batt. Pack Current Value	Amperes	(A*256+B)/100-327.68
01	5B	1	State of Charge	%	A*20/51
01	46	1	Ambient Air Temperature	°C	A-40
01	0D	1	Vehicle speed	mph	A*6213/10000
01	10	2	MAF air flow rate	grams/sec	((A*256)+B)/100